Determination of biogeochemical properties of marine particles using above water measurements of the degree of polarization at the Brewster angle.

Malik Chami[1] and David McKee[2]

[1]*Université Pierre et Marie Curie-Paris6, Laboratoire Océanographie de Villefranche, 06230 Villefranche sur Mer, France ; CNRS, Laboratoire Océanographie de Villefranche Villefranche sur Mer, France*
[2]*SUPA, Physics Department, University of Strathclyde, 107 Rottenrow, Glasgow, G4 0NG, Scotland*
chami@obs-vlfr.fr

Abstract: Retrieval of biogeochemical parameters from remotely sensed data in optically complex waters such as those found in coastal zones is a challenging task due to the effects of various water constituents (biogenic, nonalgal and inorganic particles, dissolved matter) on the radiation exiting the ocean. Since scattering by molecules, aerosols, hydrosols and reflection at the sea surface introduce and modify the polarization state of light, the polarized upward radiation contains embedded information about the intrinsic nature of aerosols and suspended matter in the ocean. In this study, shipborne above water angularly resolved visible/near infrared multiband measurements of the degree of polarization are analysed against their corresponding *in-situ* biogeochemically characterized water samples for the first time. Water samples and radiometric data were collected in the English Channel along an inshore-offshore transect. Angular variations in the degree of polarization P are found to be consistent with theory. Maximum values of P are observed near the Brewster viewing angle in the specular direction. Variations in the degree of polarization at the Brewster angle (P_B) with water content revealed that the suspended particulate matter, which is mainly composed of inorganic particles during the experiment, contributes to depolarise the skylight reflection, thus reducing P_B. An empirical polarization-based approach is proposed to determine biogeochemical properties of the particles. The concentration of inorganic particles can be estimated using P_B to within ±13% based on the dataset used. Larger sets of polarized measurements are recommended to corroborate the tendency observed in this study.

References and links

1. J. E. O'Reilly, S. Maritorena, B. G. Mitchell, D. A. Siegel, K. L. Carder, S. A. Garver, M. Kahru, and C. McClain, "Ocean color algorithms for SeaWiFS," J. Geophys. Res. **103**, 937-953 (1988).
2. J. E. O'Reilly *et al.*, "Ocean color chlorophyll a algorithms for SeaWiFS, OC2 and OC4: version 4," NASA Tech. Memo. 2000-206892, **11**, 9-27 (2000).
3. H. R. Gordon, O. B. Brown, R. H. Evans, J. W. Brown, R. C. Smith, K. S. Baker, and D. K. Clark, "A semianalytic radiance model of ocean color," J. Geophys. Res. D. **93**, 10909-10924 (1988).
4. F. E. Hoge and P. E. Lyon, "Satellite retrieval of inherent optical properties by linear matrix inversion of oceanic radiance models: an analysis of model and radiance measurement errors," J. Geophys. Res. **101**, 631-648 (1996).
5. S. A. Garver and D. Siegel, "Inherent optical property inversion of ocean color spectra and its biogeochemical interpretation 1. Time series from the Sargasso Sea," J. Geophys. Res. **102**, 607-625 (1997).

6. M. Chami and D. Robilliard, "Inversion of oceanic constituents in case I and II waters with genetic programming algorithms," Appl. Opt. **41**, 30, 6260-6274 (2002).

7. Z. P. Lee, K. L. Carder, and R. Arnone, "Deriving inherent optical properties from water color: A multi-band quasi-analytical algorithm for optically deep waters," Appl. Opt. **41**, 755-772 (2002).

8. S. Maritorena, D. A. Siegel, and A. R. Peterson, "Optimization of a semianalytical ocean color model for global-scale applications," Appl. Opt. **41**, 05-14 (2002).

9. H. Schiller and R. Doerffer, "Improved determination of coastal water constituent concentrations from MERIS data," IEEE Trans. Geosci. Remote Sens. **43**, 585-591 (2005).

10. C. H. Chang, C. C. Liu., and C. G. Wen, "Integrating semianalytical and genetic algorithms to retrieve the constituents of water bodies from remote sensing of ocean color," Opt. Express **15**, 252-264 (2007).

11. K. Y. Kondratyev, D. V. Pozdnyakov, and L. H. Pettersson, "Water quality remote sensing in the visible spectrum," Int. J. Remote Sens. **19**, 957-979 (1998).

12. R. Doerffer and J. Fischer, "Concentrations of chlorophyll, suspended matter and gelbstoff in case II waters derived from satellite coastal zone color scanner data with inverse modelling methods," J. Geophys. Res. **99**, 7457-7466 (1994).

13. C. D. Mobley, "Estimation of the remote sensing reflectance from above surface measurements," Appl. Opt. **38**, 7442-7454 (1999).

14. D. Doxaran, R. C. N. Cherukuru, and S. J. Lavender, "Surface reflection effects on upwelling radiance field measurements in turbid waters," J. Opt. A **6**, 690-697 (2004).

15. B. Fougnie, R. Frouin, P. Lecomte, and P. Y. Deschamps, "Reduction of skylight reflections effects in the above water measurement of diffuse marine reflectance," Appl. Opt. **38**, 3844-3856 (1999).

16. M. Chami, and M. Defoin-Platel, "Sensitivity of the retrieval of the inherent optical properties of marine particles in coastal waters to the directional variations and the polarization of the reflectance," J. Geophys. Res. **112**, C05037, doi:10.1029/2006JC003758 (2007).

17. M. Chami, "Importance of the polarization in the retrieval of oceanic constituents from the remote sensing reflectance," J. Geophys. Res. **112**, C05026, doi:10.1029/2006JC003843 (2007).

18. H. Volten, J. F. De Haan, J. W. Hovenier, R. Schreurs, W. Vassen, A. G. Dekker, H. J. Hoogenboom., F. Charlton, and R. Wouts, "Laboratory measurements of angular distributions of light scattered by phytoplankton and silt," Limnol. Oceanogr. **43**, 1180-1197 (1998).

19. M. Chami, R. Santer, and E. Dilligeard, "Radiative transfer model for the computation of radiance and polarization in an ocean-atmosphere system: polarization properties of suspended matter for remote sensing," Appl. Opt. **40**, 15, 2398-2416 (2001).

20. T. H. Waterman, "Polarization patterns in submarine illumination," Science **120**, 927-932 (1954).

21. T. H. Waterman, "Polarization of scattered sunlight in deep waters," Papers in Marie Biology and Oceanography, Deep Sea Res. **3**, Suppl., 426-434 (1955).

22. A. Ivanoff and T. H. Waterman, "Factors, mainly depth and wavelength, affecting the degree of underwater light polarization," J. Mar. Res. **16**, 283-307 (1958).

23. G. F. Beardsley, "Mueller scattering matrix of sea water," J. Opt. Soc. Am. **58**, 52-57 (1968).

24. B. Lundgren, and N.K. Hojerslev, "Daylight measurements in the Sargasso Sea. Results from the "DANA" expedition January-April 1966, Rep. 14, Department of physical oceanography," University of Copenhagen, Copenhagen, Denmark (1971).

25. K. J. Voss and E. S. Fry, "Measurement of the Mueller matrix for ocean water," Appl. Opt. **23**, 4427-4439 (1984).

26. J. T. Adams, E. Aas, N. K. Hojerslev, and B. Lundgren, "Comparison of radiance and polarization observed in the Mediterranean Sea and simulated in a Monte Carlo model," Appl. Opt. **41**, 2724-2729 (2002).

27. A. Cunningham, P. Wood and D. McKee, "Brewster-angle measurements of sea-surface reflectance using a high resolution spectroradiometer," J Opt. A. **4,** S29-S33 (2002).

28. J. Chowdhary, B. Cairns, M. I. Mishenko, and D. L. Travis, "Retrieval of aerosol properties over the ocean using multispectral and multiangle photopolarimetric measurements from the Research Scanning Polarimeter," Geophys. Res. Lett. **28**, 243-246 (2001).

29. J. Chowdhary, B. Cairns and L. Travis, "Contribution of water leaving radiances to multiangle, multispectral, polarimetric observations over the open ocean: bio-optical model results for case 1 waters," Appl. Opt. **45**, 5542-5567 (2006).

30. A. Gilerson, J. Zhou, M. Oo, J. Chowdhary, B. Gross, F. Moshary, and S. Ahmed, "Retrieval of chlorophyll fluorescence from reflectance spectra through polarization discrimination: modeling and experiments," Appl. Opt. **45**, 5568-5581 (2006).

31. M. Chami and R. Santer, "Aerosol remote sensing using ground based measurements and POLDER airborne sensor above coastal waters," Remote Sens. Environ. **66**, 203-221 (1998).

32. Unesco, "Determination of photosynthetic pigments in sea water," Monographs Oceanogr. Method, UNESCO **I**: 62p. (1966)

33. H. C. Van de Hulst, "*Light scattering by small particles*," (Dover, New York 1981) pp. 470.

34. G. W. Kattawar, G. N. Plass, and S. J. Hitzfelder, "Multiple scattered radiation emerging from Rayleigh and continental haze layer. 1: Radiance, polarization and neutral points," Appl. Opt. **15**, 632-647 (1976).

35. E. P. Shettle, and R. W. Fenn, "Models for the aerosols of the lower atmosphere and the effect of humidity variations on their optical properties," Environmental research papers **676**, 31 (1979).

36. J. P. Dupont, D. Bentley and A. Richard, "Suivi du détroit du Pas de Calais," J. Rech. Oceanogr. **6**, 1-16 (1981).

37. D. Bentley, "Caractéristiques physico-chimiques des eaux du Détroit du Pas de Calais," J. Rech. Oceanogr. **10** (2) :69-71 (1985).

38. J. M. Brylinski, Y. Lagadeuc, and V. Gentilhomme, "Le fleuve côtier: un phénomène hydrologique important en Manche Orientale. Exemple du Pas de Calais," Oceanol. Acta **11,** 197-203 (1991).

39. C. D. Mobley, "A numerical model for the computation of radiance distributions in natural waters with wind roughened surfaces," Limnol. Oceanogr. **34**, 1473-1483 (1989).

40. Z. Jin and K. Stamnes, "Radiative transfer in nonuniformly refractive layered media such as the atmosphere-ocean system," Appl. Opt. **33**, 431-443 (1994).

41. A. Morel and B. Gentili, "Diffuse reflectance of oceanic waters, III, Implications of bi-directionality for the remote sensing problem," Appl. Opt. **35**, 4850-4862 (1996).

42. A. Bricaud, A. Morel, M. Babin, K. Allali, and H. Claustre, "Variations of light absorption by suspended particles with chlorophyll a concentration in oceanic (case 1) waters: analysis and implications for bio-optical models," J. Geophys. Res. **103**, C13, 31033-31044 (1998).

43. H. Loisel and A. Morel, "Light scattering and chlorophyll concentration in case 1 waters: a reexamination," Limnol. Oceanogr. **43**, 847-858 (1998).

44. H. Bader, "The hyperbolic distribution of particles sizes," J. Geophys. Res. **75**, 2822-2830 (1970).

45. K. L. Carder, G. F. Beardsley, and H. Pak, "Particle size distribution in the Eastern Equatorial Pacific," J. Geophys. Res. **76**, 5070-5077 (1971).

46. E. Boss and W. S. Pegau, "Relationship of light scattering at an angle in the backward direction to the backscattering coefficient," Appl. Opt. **40**, 5503-5507 (2001).

47. D. Doxaran, J. M. Froidefond, and P. Castaing, "A reflectance band ratio used to estimate suspended matter concentrations in coastal sediment-dominated waters," Intern. Journ. of Rem. Sens. **23**, 5079-5085 (2002).

1. Introduction

Over the past two decades, ocean color data have primarily been used to infer chlorophyll concentration and phytoplankton biomass in open ocean waters. Empirical approaches, in which in situ oceanographic measurements are used to relate spectral band ratios of above surface remote sensing reflectance (Rrs) to chlorophyll a concentration ($Chla$), are generally employed for this environment [1, 2]. In recent years, there have been increasing numbers of optical studies performed in coastal waters. This is largely because a significant proportion of global marine primary production occurs on continental shelves and the coastal ocean is most utilized and impacted by humans. In coastal environments the derivation of marine biogeochemical properties from the upwelling light field can be highly inaccurate due to contributions from inorganic and/or coloured dissolved organic material. Semi-analytical algorithms, which are based on radiative transfer simulations, are used to approximate the relationship between the inherent optical properties (IOPs: absorption, scattering and backscattering coefficients) and the remote sensing reflectance. Note that model inputs often consist of the reflectance measured above the sea surface level (hereafter referred to as 0^+) because (i) the inversion algorithms are essentially devoted to ocean color satellite imagery and (ii) underwater radiometric measurements can be difficult in turbid coastal waters due to high attenuation levels. The inverse problem of ocean color in coastal zones is often examined as a two step process: derivation of IOPs from reflectance, and then biogeochemical parameters such as $Chla$ or suspended particulate matter (SPM) concentration from the IOPs. Numerous retrieval algorithms based on the semi-analytical approach have been developed [3-11]. For example, Rrs can be inverted via various optimisation techniques [7,8] such as the Levenberg-Marquart approach [11] and nonlinear least square schemes [5] or via a modification of the inverse problem to a simplified expression for linear inversion such as the simplex method [12] or the matrix inversion based on the least-squares approach [4].

Beyond retrieval errors due to the particular algorithm employed, current inversion techniques have two other limitations. First, estimation of remote sensing reflectance from above surface measurements such as the downwelling irradiance E_d and water leaving radiance L_w can be significantly affected by errors associated with removal of surface-reflected sky radiance [13,14]. In particular, the sea surface Fresnel reflectance factor (which

is used to remove the reflected sky radiance) is strongly dependent on the windspeed and solar zenith angle. Second, most of the current algorithms developed for coastal waters focus on the retrieval of IOPs rather than biogeochemical parameters. The principal reason for that is the lack of reliable bio-optical models that relate the IOPs to the suspended particulate material in those areas. Therefore, assessment of particulate fluxes in the coastal ocean and investigations into the transport and fate of sediments and pollutants on continental shelves, which are of great interest for coastal zone management and other policy decisions, still remain difficult to perform.

Previous studies have investigated the use of the polarization state of light to overcome some of the limitations mentioned above [15-17]. Based on the theoretical finding that the specular reflection of the sky radiance at the air-sea interface is totally perpendicularly polarized at the Brewster viewing angle θ_B ($\theta_B = 53.2°$ for the air-sea interface), Fougnie et al. [15] proposed to significantly reduce the contribution to reflectance from skylight reflection by measuring the parallel component of the upwelling signal. The underlying assumption is that the radiance scattered by the ocean does not significantly alter the polarization state of light at 0^+. Note that Fougnie et al. [15] focused their study on open ocean waters only. Other investigators [18,19] suggested that polarization measurements could be used to separate the fraction of inorganic particles from biogenic cells. Recently, Chami [17] showed based on theoretical modelling that an empirical-based inversion approach relying on the underwater polarized reflectance could retrieve the concentration of inorganic particles regardless of the phytoplankton content in coastal waters. On this basis, measurement of the polarization state of oceanic radiation might allow direct estimation of suspended inorganic matter concentration from remotely sensed data in coastal areas.

Despite the importance of polarization for marine applications, relatively few in-situ observations of the oceanic polarization state of light have been carried out [20-30] owing to a lack of instrumentation and to the practical difficulties in achieving reliable measurements. It is the purpose of this paper to exploit unique shipborne above water angularly resolved measurements of the degree of polarization obtained in a coastal environment to derive biogeochemical properties of the water mass. Another goal of this paper is to validate some of the theoretical findings about the influence of marine particles on the polarized signal. Note that it is the first time, to our knowledge, that in-situ angularly resolved polarized radiometric measurements at 0^+ have been collected at various viewing angles and analyzed. The paper is organized as follows. First, the field experiment will be described. Then measurements of the degree of polarization will be presented and discussed together with in-situ biogeochemical data. In particular, we will focus on variations in the degree of polarization measured at the Brewster angle with respect to suspended particulate material concentrations. The results will be interpreted using radiative transfer modelling.

2. Data and methods

Data were collected during a field experiment in the English Channel in summer 1994. The study area and the conditions of the cruise experiment were described in detail in Chami and Santer [31]. Radiometric and biological measurements were collected onboard the research vessel Sepia II (Centre National de la Recherche Scientifique, France) along an inshore-offshore transect located in the Strait of Dover (see Fig. 3 in [31]). The data reported in this paper were recorded at nine stations on June 14 1994 in the morning (between 9 am and 2 p.m UTC). The coordinates of each station are given in table 1. Note that stations 1 and 9 were located near the coast and the middle of the Strait respectively. The distance between sampling stations was about 0.6 nautical miles up to station 7 and about 1.2 nautical miles from station 7 to station 9. The maximum depth of the Strait of Dover is about 50 m.

Table 1 : Coordinates of the sampling stations

Station	Latitude	Longitude
1	50°47.70N	1°33.90E
2	50°47.85N	1°32.80E
3	50°47.85N	1°31.80E
4	50°48.05N	1°31.00E
5	50°48.10N	1°29.75E
6	50°48.30N	1°29.00E
7	50°48.50N	1°27.10E
8	50°48.90N	1°24.30E
9	50°49.30N	1°22.50E

2.1 Biogeochemical measurements

Water samples (18 in total) were taken at two depths (surface and bottom) using a 5 L Niskin bottle. For analysis of phytoplankton pigments and particulate concentrations, suspended particles were filtered from water samples onto Whatman glass-fiber filters (GF/F). The filters were then stored in liquid nitrogen before analysis in the laboratory. The spectrophotometric method was used to estimate *Chla*. In this method the optical density (absorbance) of pigment extracted in ethanol was measured at 665 nm. After correction for background signal in the near infra red (750 nm), the absorbance was converted to *Chla* using the relationships established by Unesco [32]. The concentration of total (*SPM*), inorganic (*IPM*) and organic (*OPM*) particulate matter was also measured. To estimate the total suspended matter concentration, the GF/F filters were weighed before and after filtration of water samples. The inorganic particulate matter was derived by burning the total suspended matter and weighing the residue. The organic particulate matter concentration was obtained by difference between *SPM* and *IPM*. *In-situ* vertical profiles of physical properties of seawater including temperature and salinity were measured using SeaBird temperature, conductivity and pressure sensors.

2.2 Measurements of the degree of polarization

Polarized light can be described by the four Stokes parameters (see [33] for details). Since the ellipticity of the radiance generated by natural processes has been shown to be negligible [34], three parameters are sufficient to describe the polarization state of reflected light : (i) the total reflectance which is the sum of unpolarized and polarized light, (ii) the polarized portion of the total reflectance (i.e., polarized reflectance) and (iii) the angle of the linear polarization relative to the vertical reference plane (containing the viewer). The degree of polarization P is defined as the ratio of the polarized reflectance to the total reflectance. The degree of polarization of scattered light can be expressed as [Eq. (1)]:

$$P = \frac{I_{\perp} - I_{II}}{I_{\perp} + I_{II}} \tag{1}$$

where $I_{\perp}$ represents the flux of scattered light polarized perpendicular to the reference plane and $I_{//}$ represents the flux of scattered light polarized parallel to the reference plane.

An instrument, called REFPOL, was developed at the Laboratoire d'Optique Atmosphérique, (University of Lille, France) for measuring the bidirectional polarization distribution function of the atmosphere and surfaces in the field. It was equipped with 4 optical barrels, each carrying a different spectral filter. During the English Channel cruise, the 4 channels were centered at 450 nm, 650 nm, 850 nm and 1650 nm with passbands of 100 nm for the 1650 nm band, and 40 nm for the others. Polarizers rotate in front of the 4 detectors (3 silicon photodiodes and one germanium for the longest wavelength band) and allow three successive measurements with three polarizers turned by steps of 45°, thus providing the degree of polarization. Calibration of the REFPOL instrument was performed before and after the field campaign in the laboratory using an integrating sphere. The radiometric uncertainty

was of the order of ±5%. Note that one of the major advantages of the degree of polarization is that it is less sensitive to calibration errors than is the absolute radiance.

The radiometer was mounted on a scanning system operating twice (one way and back) through a 2π cycle scanning in a vertical plane. A step by step electric engine allowed an inclination up to 70° either side of nadir viewing. Measurements were made every 2.5°. An inclinometer automatically provided the zenith viewing angle of the radiometer and this information was stored with the measurements. The total angular sampling time from –70° to +70° was 120 seconds. REFPOL was mounted at the extremity of the front deck of the ship (~ 10 m height) in such a way that the observation plane was nearly perpendicular to the ship axis. The field of view was 16° (total) which yielded a footprint size of 2.8 m. By rotating from –70° to +70° relative to the nadir direction, the radiometer sampled the angular signature of the degree of polarization of the water surface in a vertical plane defined by its azimuth angle relative to the sun. The azimuth angle could be changed easily by hand. However, the measurements were collected exclusively in the principal plane, which is defined by the sun zenith and observation direction. Thus, the principal plane corresponded to the reference plane. In this paper, a positive value of the viewing zenith angle θ_v specifies view rays from the sensor that reflect toward the sun (termed "specular direction"), while negative values of θ_v mark view rays that reflect away from the sun (termed "anti-specular direction") (Fig. 1). Note that, when looking upwards, the instrument measured the skylight polarization which is a separate portion of the entire measurement sequence. Here, since our goal is to examine the influence of the subsurface suspended particles on the degree of polarization, we focus on analysis of REFPOL data when the instrument was looking at the sea surface at the three spectral bands that are of interest for ocean color studies, namely 450 nm, 650 nm and 850 nm. The windspeed was about 2 m s^{-1} resulting in a calm flat sea with negligible wave structure effects.
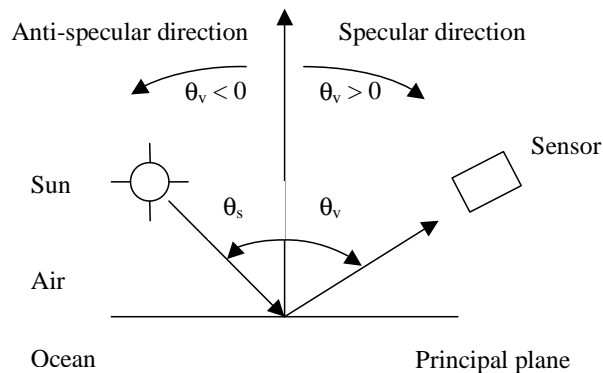

Fig. 1. Geometry of observation of the REFPOL instrument in the principal plane.

3. Results and discussion

The environmental conditions observed during the field experiment were previously described in [31]. The solar zenith angle θ_s varied from 28° to 39° along the transect (table 2). Since the measurements started from the coast, the solar zenith angle was greater at the first station and decreased as the ship moved offshore. The atmosphere was relatively turbid. The aerosol optical depth at 550 nm, which was measured using a Cimel radiometer, ranged from 0.4 to 0.9 over the course of the day, which is equivalent to horizontal visibility in the range 8 km – 15 km. The atmospheric turbidity was relatively stable during the morning of the transect (table 2) and continuously increased in the afternoon together with the relative humidity. Both parameters (i.e., aerosol optical depth and humidity) showed the highest values around 4 pm

(UTC). Rigorous analysis of REFPOL skylight polarization measurements revealed that the Shettle and Fenn model T90 [35] correctly matched the aerosol optical properties on June 14 1994 [31]. Furthermore, the spectral variation of the aerosol optical depth was stable in the morning (the Angstrom exponent was about 1.6, see Fig. 5 in [31]), suggesting that the optical properties of the aerosols changed slightly during the period of data collection.

Table 2. Time (in UTC), solar zenith angle θ_s (in degrees) and aerosol optical depth τ_a measured at 550 nm during the transect on June 14 1994.

Station	1	2	3	4	5	6	7	8	9
Time	9.3 am	9.7 am	10.0am	10.5am	10.8am	11.3am	11.4am	12.4pm	1.1pm
θ_s	38.9	37.7	34.9	32.0	30.7	28.5	27.8	28.1	31.0
τ_a(550 nm)	0.38	0.38	0.36	0.37	0.40	0.44	0.45	0.49	0.50

3.1 Chlorophyll a and suspended particulate matter concentrations

Figure 2 shows surface horizontal gradients of *Chla* and suspended particulate matter concentrations (i.e. *SPM, IPM, OPM*) along the transect. The general trend is a decrease in particle loading from the coast heading offshore. The chlorophyll *a* concentration varies from 1.6 to 8.5 mg m^{-3}. The highest value is observed at station 2. The slope of the decrease in *Chla* is steepest in the first part of the transect between stations 2 and 5 where *Chla* drops by a factor of 2. The horizontal variations of the other particulate parameters have similar features to those observed for *Chla*. High concentrations of suspended material near the coast are consistent with increases in terrigenous inputs due to the strong influence of continental effects such as river runoffs. The strong gradient observed between stations 2 and 5 indicates that coastal waters are clearly dissociated from the open ocean. Previous studies carried out in the same area [36-38] demonstrated the occurrence of a quasi permanent frontal zone that separates the coastal and open ocean water types, the effect of which is to prevent the migration of particles away from the coast. Brylinsky et al. [38] highlighted that the front induces a meridional flow of the coastal current along the continent. The physical properties of the water mass (i.e., density, salinity and temperature) measured by the CTD (Conductivity Temperature Depth sensors) are consistent with the occurrence of the front during the experiment. The temperature and salinity are respectively higher and lower near the coast. The density gradient is strongest at station 5, suggesting that the frontal zone is located near this station. CTD measurements also reveal homogenous vertical profiles of the density for each station, meaning that the water masses are well mixed. Vertical profiles of particulate concentrations are fairly homogenously distributed in the water column due to resuspension of particles from the bottom to the surface layer.
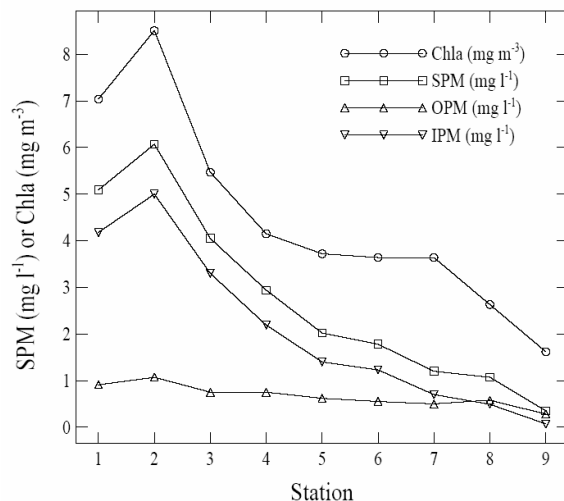
Fig. 2. Variations in the suspended matter (organic, inorganic and total suspended matter) and *Chla* concentrations along the transect.

Figure 2 also shows that the concentration of inorganic particles is much greater than that of organic particulate matter, except for the two furthest offshore stations (stations 8 and 9). The contribution to the total particulate matter from inorganic particles is often significant along the transect, exceeding 50% in coastal stations (Fig. 3). Note that the inorganic particles dominate by more than 70% the samples collected upstream from the frontal zone. Therefore, despite a significant concentration of phytoplankton and biological activity, minerals still remain the main contributor to the particulate material for most of the stations of the transect. On the other hand, the organic particles contribute about 60%-80% of the total suspended matter for the offshore stations located beyond the front (station 8 and 9) which are the clearest as well. Note that the organic particulate matter concentration is almost constant along the transect. Thus, *OPM* cannot be a significant source of variability in optical signals for these stations.
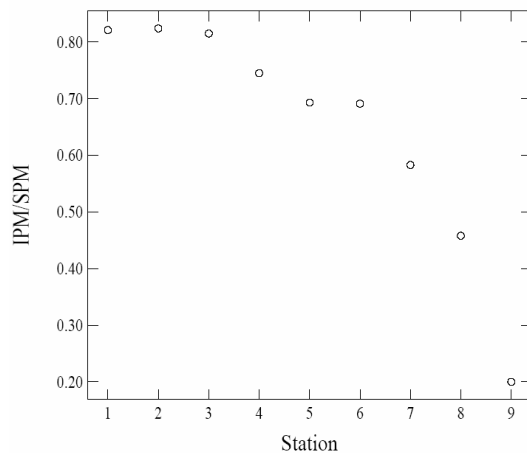

Fig. 3. Variations of the portion of inorganic particles (i.e., *IPM/SPM*) along the transect.

3.2 Above surface measurements of the degree of polarization

The angular distribution of the degree of polarization measured at 650 nm above the sea surface is first examined for various stations along the transect (Fig. 4). Angular variations in the degree of polarization show similar features for each station. P is highly peaked in the specular (i.e., $\theta_v > 0$) and anti-specular directions (i.e., $\theta_v < 0°$) around $\theta_v = 55°$ and P shows a minimum value around the nadir viewing angle. Note that the peak produced in the anti-specular direction is slightly less pronounced than that observed in the specular direction.
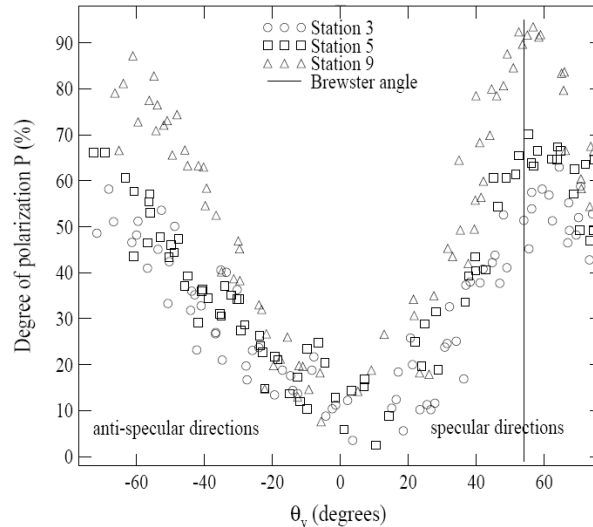

Fig. 4. Angular variations in the degree of polarization measured at 650 nm at 0^+ for various stations along the transect : station 3, 5 and 9. Note that the half-plane where $\theta_v > 0$ is the specular direction and the half-plane where $\theta_v < 0$ is the anti-specular direction.

For both the specular and anti-specular directions, maximum values of P are observed close to the Brewster angle θ_B, which is $\theta_B = 53.2°$ when dealing with a flat sea surface. On the basis of the Fresnel's law, the Brewster angle is an interesting singular point for the polarization field as the reflected skylight radiation is theoretically totally perpendicularly polarized in this geometry, the parallel component (i.e., $I_{//}$) becoming identically zero. Thus, the degree of polarization is maximised and theoretically reaches 100% at the Brewster angle. However, it is often less than 100% in natural waters, as observed in Fig. 4. Different processes potentially contribute to the value of $P(\theta_B)$ (hereafter referred to as P_B). First, agitation of the ocean surface caused by wind contributes to a natural depolarization. Here, because of the weak windspeed, a slight depolarization (a few percent) is expected. Second, the net degree of polarization emanating from the ocean surface is complicated by the emergence of light from below the air-water interface due to scattering of incident radiation by particles in the water. In particular, P_B decreases as the turbidity increases near the coast, suggesting that the degree of polarization measured at the Brewster angle might provide information on water content. The influences of marine particles on P_B will be discussed later.

To compare our measurements with theory, radiative transfer computations of the above water degree of polarization are carried out. The simulations are made using the OSOA model [19]. The OSOA radiative transfer model is appropriate here since it accounts for the polarization state of light in the coupled ocean-atmosphere system, which is not the case for most of the commonly used radiative transfer codes such as Hydrolight [39], CDISORT [40] or Monte Carlo [41]. The simulations are performed for the offshore station case (station 9) which shows the highest peaks of P. The input parameters of the model are based on atmospheric and oceanic observations. The Shettle and Fenn aerosol model T90, which was

derived from REFPOL skylight measurements [31], and the measured aerosol optical depth (table 2) are used to simulate the incoming solar light. The solar zenith angle is θ_s=31°. The *Chla* and total suspended particle concentrations are 1.6 mg m^{-3} and 0.4 mg l^{-1} respectively. The absorption and scattering coefficients of phytoplankton are derived from *Chla* using the bio-optical models of Bricaud et al. [42] and Loisel and Morel [43]. Phytoplankton and inorganic particles phase functions are modelled using Mie theory. The refractive indices of phytoplankton and inorganic matter relative to water are set to 1.05 and 1.18 respectively. The size distribution of particles is assumed to follow the Junge hyperbolic function, which is often used for natural waters [44-46], with a Junge exponent value of –4. The minimum and maximum radii of the size distribution are 0.1 μm and 50 μm respectively. Homogenous vertical profiles of hydrosols are considered since the waters were well mixed. Figure 5 shows the comparison between measurements and model outputs. The model nicely reproduces the observed angular variations in *P*. It is noteworthy that the measurements are highly consistent with theory in the anti-specular direction. Note that the simulated results are weakly sensitive to variations in the refractive indices or the Junge exponent due to the low concentration of suspended particles in the water mass at station 9. The good agreement observed between radiative transfer modeling and the radiometric measurements indicate *a posteriori* that the quality of the *in-situ* data is fairly satisfactory despite the practical difficulties relative to shipborne measurements.

To gain an understanding of the influence of the atmosphere on the degree of polarization, computations are repeated with and without atmosphere, for which aerosol and molecule optical depths are set to zero (Fig. 5). When the atmosphere is ignored in the computations, the angular variation in the degree of polarization is fairly flat in the anti-specular direction where *P* is very weak in magnitude. The comparison between the two simulated cases corroborates the argument that differences in depolarization between specular and anti-specular angles, which already depend on water leaving radiance, are also a function of contributions from direct reflection. Direct reflection is notably stronger in specular directions than in anti-specular directions since the forward-scattered sky radiance driving the specular directions is stronger than the back-scattered sky radiance driving the anti-specular directions. Also, at the Brewster angle, the direct reflectance component is highly polarized. Therefore, even if the water leaving component is the same for both anti and specular directions, the fact that the direct reflection is considerably stronger in the specular direction means that the depolarization from the water leaving component is a smaller percent effect than for the anti-specular direction. In the anti-specular direction, the direct reflection is relatively smaller, and the depolarization is relatively more important. For the extreme case where the atmosphere is omitted in the simulation, the direct reflection is null for the anti-specular direction, there being no sky radiation for the interface to polarize. In the specular direction, the predicted degree of polarization at the Brewster angle for the case without atmosphere is slightly lower than with atmosphere because for the latter case, the additional scattered light adds to the direct solar beam, increasing the surface reflection component. Note that the occurrence of any signal in the specular direction for the without-atmosphere case is due to sea surface waveslopes differing from zero due to Cox-Munk model with 2 m s^{-1} windspeed. Although the maximum radiance reflection would occur at the specular angle θ_s (31 deg in this case), the maximum degree of polarization would occur at Brewster angle, corresponding to a waveslope of about 7.5 deg.
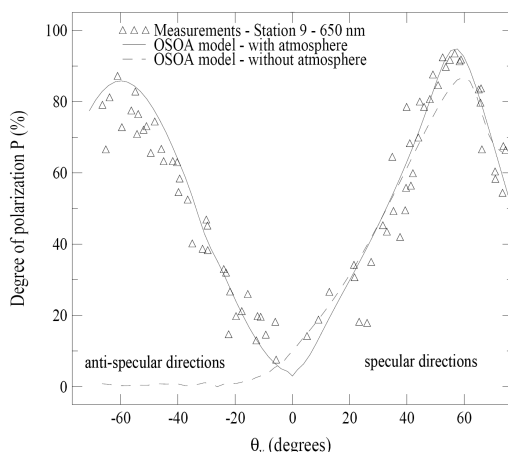
Fig. 5. Angular variations in the degree of polarization measured at 0^+ at 650 nm at the offshore station 9. The measurements are compared with radiative transfer simulations. The inputs of the radiative model are outlined in the text.

3.3 Spectral variation in the degree of polarization

Variations in the degree of polarization with wavelength are now studied. First, the measurements collected at the offshore station 9 are examined. Figure 6 shows the angular distribution of P at 450 nm and 850 nm. Note that the measurements collected at 650 nm were previously plotted in Fig. 5. One of the most striking features is that the peaks observed in both half spaces are more pronounced as the wavelength increases. As an example, P_B varies from 84% to 100% between 450 nm and 850 nm. Similarly, the maximum observed in the anti-specular direction varies from 64% to 98%. For observations at a given station, decreases in the magnitude of P are due to the increased level of scattering from beneath the surface with decreased wavelength. This in turn is due to substantially larger subsurface illumination levels thanks to less absorption at decreased wavelengths (water absorption coefficient of 0.01 m^{-1} at 450 nm versus 2 m^{-1} at 870 nm), along with some Rayleigh scattering (Rayleigh scattering attenuation coefficient of 0.0015 m^{-1} in pure water at 550 nm). The increased level of water leaving radiance competes vectorially with the above water reflected skylight, thus inducing a significant depolarisation of the upward radiation. At 850 nm, the magnitude of the subsurface radiation is lower than in the blue due to both the increased absorption and lower scattering by water molecules. Thus, the subsurface radiation has little influence on the above water polarization field and the upward signal is completely polarized at both θ_B and θ_v=-55° due to surface reflection phenomena. Figure 6 also shows the consistency of spectral multi-angular measurements with simulations. Inputs similar to those used for the retrieval of P at 650 nm were used for the OSOA radiative transfer model. The agreement between measurements and theory is very satisfactory, and demonstrates our ability to reproduce multiband above water polarization measurements from knowledge of atmospheric and oceanic parameters.
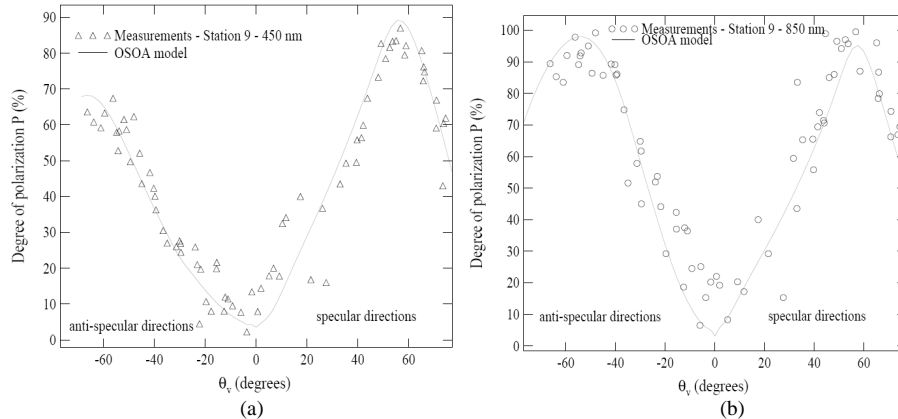
Fig. 6. Angular variation of the degree of polarization (a) at 450 nm and (b) 850 nm. Radiative transfer computations are also added (see text for the description of the model inputs).

Spectral variations in P_B measured at different coastal stations are plotted in Fig. 7 and compared to the offshore station (station 9). A decrease of P_B toward short wavelengths is systematically observed for each station as a result of increased scattering from subsurface suspended particles due to increased subsurface illumination levels. Consequently, increased suspended particle loadings will result in increased water leaving radiance, further depolarisation, and in turn lower P_B. P_B significantly decreases for stations located closer to the shoreline. For example, P_B varies from 84% to 45% in the blue from the offshore to the inshore stations. It is interesting to note that the magnitude of the degree of polarization at station 1 significantly departs from 100% at 850 nm (~80%). Since the atmospheric turbidity was weakly variable along the transect, especially between station 1 and 4 (table 2), the sensitivity of P_B to the station location is broadly attributable to the concentration of particulate matter in the water mass, which is much higher for coastal stations (Fig. 2). The sensitivity of P_B to suspended matter concentration is studied in the following section.
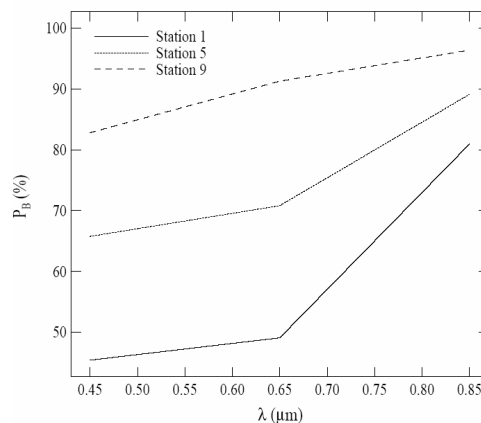

Fig. 7. Spectral variation of the degree of polarization P_B measured at the Brewster viewing angle at various stations, namely station 1, 5 and 9.

3.4 Relationships between the degree of polarization measured at the Brewster angle and suspended matter concentrations

As discussed above (Fig. 4 and Fig. 7), the degree of polarization at 0^+ is highly sensitive to the turbidity of the water mass, especially at the Brewster viewing angle θ_B. Therefore, it

might be possible to exploit measurements of P_B in coastal waters to derive information about water content such as the concentration of the particles. Relationships between P_B and the concentration of suspended matter are now investigated. Since the range of variation of P along the transect is greater at 650 nm than at other wavelengths (Fig. 7), variations in P_B with the water turbidity are studied at 650 nm. Note that the use of a red wavelength is convenient to reduce the contribution of water molecules to the degree of polarization and to enhance the signature of the subsurface particles. Figure 8 shows the relationships obtained between P_B at 650 nm and concentrations of *SPM* and *IPM*. The general trend is a significant decrease in P_B as the particle loading of the water mass increases. As expected, a high value of P_B (~90%) is observed in clear waters (i.e., $SPM = 0.4$ mg l^{-1}) because of the dominant contribution to the reflectance from the skylight reflection at the interface compared to the contribution from the signal exiting the ocean. This result supports the approach suggested by Fougnie et al. [15] which consists of using the polarized signal at the Brewster angle in clear waters to correct for above water radiances from the skylight reflection. When the turbidity increases, the amount of transmitted light through the boundary significantly increases. Despite a very weak polarization of the transmitted radiation due to the interface, the vectorial addition of the transmitted light and the reflected skylight radiation reduces the polarization level of the signal measured at 0^+. The recommendation to observe the ocean through a vertical polarizer to avoid strong skylight perturbation, as proposed by Fougnie et al. [15], may still be applied in turbid waters. However, the polarization factor that is used in Fougnie's approach to convert the parallel-polarized reflectance to unpolarized reflectance should be carefully estimated in coastal waters to account for the polarization effects induced by ocean constituents. Currently, the polarization factor is calculated theoretically for open ocean conditions [15]. This study shows that the polarization factor needs to be adjusted for turbid waters. Such a task is challenging because of the strong variability of the composition of the particles found in those areas, which makes difficult the selection of an appropriate model of hydrosol (i.e., refractive index and size distribution) to compute the polarization factor.
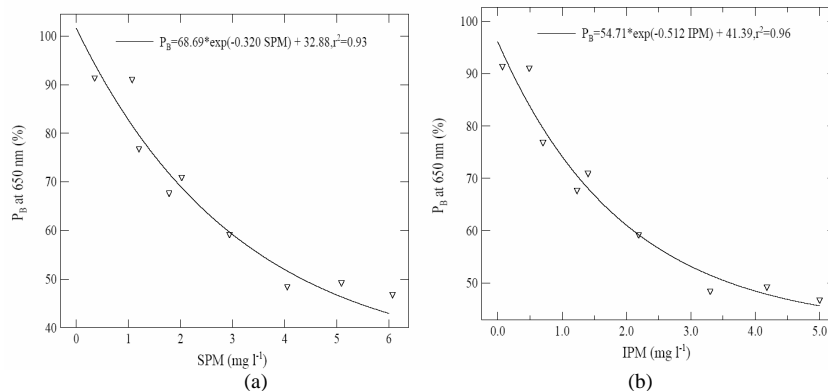

Fig. 8. Relationship between the degree of polarization measured at the Brewster angle P_B at 650 nm and (a) total suspended matter concentration *SPM* and (b) inorganic suspended matter concentration *IPM*. The best fits and the coefficient of determination r^2 have been added in the figures.

The best fits for the empirical relationships found between P_B and the particulate concentrations show that the degree of polarization decreases exponentially with turbidity (Fig. 8). The significant correlation obtained between the degree of polarization and the total suspended matter concentration *SPM* (r^2=0.93) [Fig. 8(a)] suggests that this latter parameter can be realistically retrieved from the polarization pattern measured above the sea surface using a straightforward empirical relationship. Figure 8(b) shows that inorganic matter explains 96% of the observed variability in P_B. Therefore, inorganic material is the main source of variability in the polarization signal. Such a result was expected here since the dynamic observed for *IPM* and *OPM* is very different. During the experiment, *IPM* varies by

a factor of 50 (i.e., from 0.1 to 5 mg l^{-1}) while *OPM* varies by a factor of 3 only (from 0.3 to 1.1 mg l^{-1}). *OPM* is nearly constant compared to the *IPM* dynamic (Fig. 2). On this basis, the set of measurements presented in this study is not sufficiently representative to be generalized for global observation. Measurements made in areas where *OPM* is the main contributor to the total suspended matter are necessary to confirm the observed trend. However, based on previous theoretical findings [19] which showed that the magnitude of the signal that is ascribed to biogenic material is about one order of magnitude lower than the signal ascribed to highly refractive particles at long wavelengths, the influence of *OPM* on the degree of polarization in the red is expected to be much lower than that of *IPM*. Our field results are consistent with these theoretical findings.

3.5 Determination of particulate concentrations from the degree of polarization measured at the Brewster angle

Since inorganic particles have the major impact on the degree of polarization for our dataset, an attempt is made to retrieve their concentration from remotely sensed polarized measurements at 650 nm. Thus, the relationship obtained in Fig. 8(b) is inverted to express *IPM* as a function of P_B [Fig. 9(a)]. The concentration of inorganic matter could be derived from P_B using Eq. (2)

$$IPM = 1.469 \, \mathrm{Ln}(P_B - 44.498) + 5.957 \qquad (2)$$

where the units of *IPM* and P_B are mg l^{-1} and percents respectively. Note that the coefficient of determination of the *IPM*-P_B relationship is $r^2 = 0.96$.

A simple way to evaluate the errors induced on *IPM* due to the proposed empirical algorithm consists of comparing the inorganic particulate matter concentration estimated using Eq. (2) (hereafter referred to as *IPM$_{estimated}$*) with the measurements (hereafter referred to as *IPM$_{measured}$*) [Fig. 9(b)]. Note that this analysis provides an indication of the errors and should not be seen as a rigorous validation exercise. The error in the retrieval of *IPM* is calculated using the relative root mean square error (*RRMSE*) which is defined as Eq. (3):

$$RRMSE = \sqrt{\frac{1}{n}\sum_{i=1}^{n}\left(\frac{IPM_{iestimated} - IPM_{imeasured}}{IPM_{imeasured}}\right)^2} \qquad (3)$$
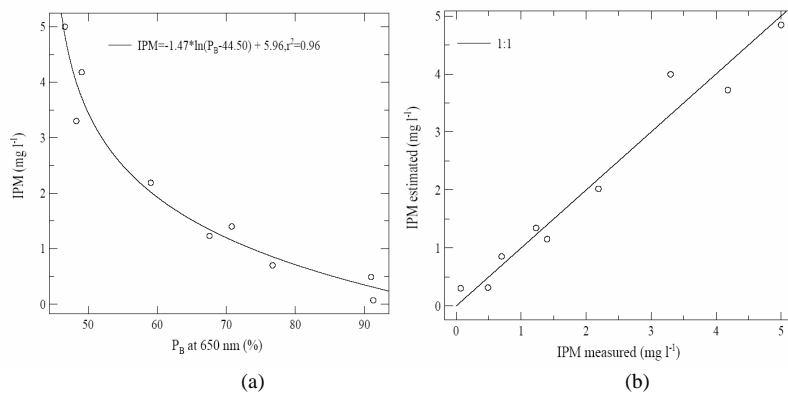
where *n* is the number of measurements.

Fig. 9. (a). Relationship between the inorganic particulate concentration *IPM* and the degree of polarization measured at Brewster angle at 650 nm P_B, (b) comparison between *IPM* retrieved from the empirical algorithm [Eq. (2)] and the measurements.

The overall relative error in the estimates of *IPM* from the degree of polarization measured at the Brewster angle is 13.0 %, which is satisfactory. These results indicate that a straightforward empirical polarization-based algorithm could be useful for deriving mineral

concentrations in local coastal applications, supporting the theoretical analysis recently presented by Chami [17]. Further radiative transfer simulations showed that the relationships between *IPM* and P_B are highly dependent on the solar zenith angle and atmospheric conditions (optical depth, aerosol model). In practice, P_B measurements would need to be adjusted for skylight conditions per the radiative transfer model computations in order to estimate *IPM* for data collected under a wide range of atmospheric conditions and solar zenith angles. The results obtained in this study are encouraging given the optical complexity of the coastal waters, but the method needs to be examined on larger datasets in the future.

The polarization-based empirical algorithm is a complementary attractive approach to the radiance-based empirical algorithms which currently make use of the radiance signal in the near infra red spectrum to derive *SPM* in coastal waters [47]. Nevertheless, such an approach is sensitive to the roughness of the sea surface and thus to the windspeed. For significant windspeeds, surface waves will change the polarization pattern. *P* will have values somewhat above or below its calm water value, depending on the slope of the waves, but *P* will be still highly influenced by the particulate loading. It is likely that the parameters of the relationships obtained between P_B and *IPM* [Eq. (2)] in this study have to be adapted for such conditions.

4. Conclusion

Above water measurements of the degree of polarization were acquired during a field experiment in the English Channel. In the first part of the paper, a rigorous analysis of the angular variations in the degree of polarization was performed since this is the first time, to our knowledge, that such shipborne above water measurements have been made. It was observed that the shape of the degree of polarization *P* is fairly symmetric around the nadir viewing angle (θ_v=0°). *P* reaches maximum values for both the specular and anti-specular directions at the Brewster viewing angle (i.e., θ_B=53.2°). These features were attributed to the effects of Fresnel reflectance. The downwelling light already scattered by the atmosphere in these directions is reflected by the sea surface which polarizes the upward radiation. This polarizing effect is amplified around the Brewster viewing angle. The measurements were highly consistent with theoretical radiative transfer simulations. Spectral variations in the degree of polarization showed a decrease toward short wavelengths due to the increased level of water leaving radiance.

In the second part of the paper, variations in *P* with water content were investigated. The degree of polarization was highly sensitive to the amount of light transmitted from beneath the surface (i.e., marine reflectance) which is strongly correlated to the water turbidity. Therefore, polarized measurements above the sea surface for correcting the upward radiance for skylight reflection effects as proposed by other investigators [15] should be carefully processed when dealing with coastal turbid waters. An original empirical polarization-based approach was proposed to determine the concentrations of suspended particles. Because the *in-situ* data used here are a limited set for which the marine reflectance variation is primarily governed by inorganic matter content, the degree of polarization measured at the Brewster angle (P_B) was related to the inorganic particle concentration. P_B allows retrieval of the inorganic particulate concentration within ±13% in the study area, which is satisfactory given the optical complexity of these coastal waters. Nevertheless, it should be highlighted that a restricted set of measurements (corresponding to calm sea state and for coastal waters where *SPM* is dominated by *IPM*) was used to derive the empirical algorithm. So for example, because the sea state affects the viewing angle, the roughness of the sea has to be considered to build appropriate empirical algorithms. Although this study covered limited optical conditions of natural seawater, we were able to demonstrate that the polarization based empirical approach could be used as an alternative method to derive biogeochemical properties of the water mass from remotely sensed data. The advantages of the method proposed here are as follows. The polarization-based approach (i) is readily implemented in terms of instrumentation, and (ii) is weakly dependent on instrument calibration since the degree of polarization is a ratio.

The empirical polarization algorithm, which consists of a simple nonlinear relationship, might with further efforts be applied to satellite sensors measuring the polarization state of

light such as the PARASOL sensor (CNES) to derive suspended matter concentration. Note, however, that in this latter case, the atmospheric correction over coastal waters needs to be accurately carried out, which still remains a challenging task due to significant effects of aerosols on the polarization state of light. Analysis of directional variations in the degree of polarization as measured by the PARASOL sensor will allow a synoptic view of the biogeochemical properties of particles in coastal zones. Mapping biogeochemical parameters such as mineral concentration in the coastal ocean from satellite data is of great interest for estimating suspended matter fluxes between continents and the ocean which are key to predicting local impacts of climate changes and anthropogenic factors on coastal and shelf seas. Future efforts should also be put into the development of in-situ instruments measuring the polarization state of light to improve the empirical relationships obtained in this study.

Acknowledgments

Notation and abbreviation

$Chla$	Chlorophyll a concentration (mg m^{-3})
E_d	downwelling irradiance (W m^{-2})
$I_\perp$	Flux of the scattered light polarized perpendicular to the scattering plane
$I_{//}$	Flux of the scattered light polarized parallel to the scattering plane
L_w	water leaving radiance (W m^{-2} sr^{-1})
0^+	above the sea surface
P	Degree of polarization above the sea surface (%)
P_B	Degree of polarization at Brewster viewing angle θ_B=53.2°
θ_B	Brewster viewing angle: θ_B=53.2°
θ_s	Solar zenith angle (degree)
θ_v	Viewing angle (degree)
τ_a	aerosol optical depth
CNES	Centre National d'Etudes Spatiales
CTD	Conductivity Temperature Depth
IOP	Inherent Optical Properties
IPM	Inorganic particulate matter concentration (mg l^{-1})
OPM	Organic particulate matter concentration (mg l^{-1})
OSOA	Ordres Sucessifs Ocean Atmosphere
PARASOL	Polarization and Anistropy of Reflectances for Atmopsheric Sciences Coupled with Observations from a Lidar
REFPOL	REFlectance POLarimeter
RRMSE	Root Mean Square Error [see Eq. (3)]
Rrs	Remote sensing reflectance (sr^{-1})
SPM	Total suspended particulate matter concentration (mg l^{-1})